J. Synchrotron Rad. (1997). **4**, 298–310

Anomalous Dispersion with Edges in the Soft X-ray Region: First Results of Diffraction from Single Crystals of Trypsin Near the *K*-Absorption Edge of Sulfur

S. Stuhrmann,[a]† K. S. Bartels,[a] W. Braunwarth,[a] R. Doose,[a] F. Dauvergne,[b] A. Gabriel,[b] A. Knöchel,[c] M. Marmotti,[a] H. B. Stuhrmann,[a]*‡ C. Trame[a] and M. S. Lehmann[d]

[a]GKSS Forschungszentrum, D-21502 Geesthacht, Germany, [b]European Molecular Biology Laboratory, Heidelberg, Outstation Grenoble, F-38042 Grenoble, France, [c]Institut für Anorganische Chemie und Angewandte Chemie, Universität Hamburg, D-20146 Hamburg, Germany, and [d]Institut Max von Laue–Paul Langevin, BP 156X, F-38042 Grenoble, France. E-mail: stuhrmann@godot.ibs.fr

(*Received 31 January 1997; accepted 17 June 1997*)

Anomalous dispersion of X-ray diffraction at wavelengths near the X-ray *K*-absorption edge of sulfur at wavelengths around 5 Å has been applied to single crystals of trypsin obtained from an ammonium sulfate solution. The multiwavelength anomalous-dispersion method based on 775 unique reflections (+183 Bijvoet mates) measured at three wavelengths near the *K*-absorption edge of sulfur in trypsin (two methionines and disulfide bridges of six cystines) reproduces the known features of the trypsin structure at a resolution of 4 Å. It appears that there is anisotropic anomalous scattering from the disulfide bridges of cystine. The multiwavelength anomalous solvent contrast shows up at wavelengths near the *K*-absorption edge of the sulfate ions, which is shifted by 10 eV to higher energies with respect to that of sulfur in trypsin. The influence of the complex contrast of trypsin in 2.5 *M* ammonium sulfate on the dispersion of a low-order reflection is analyzed. The measurement of anomalous dispersion of X-ray diffraction at long wavelengths beyond 5 Å requires a special diffractometer, the features of which are presented. An outstanding one is a detector system consisting of four multiwire proportional counters. Its efficiency is compared with that of imaging plates. The influence of radiation damage with soft X-ray diffraction from single crystals of trypsin is presented and possible remedies are discussed.

Keywords: multiwavelength anomalous dispersion; sulfur; trypsin; soft X-ray diffraction; anisotropic anomalous scattering; radiation damage.

1. Introduction

In structure analysis by X-ray diffraction the X-ray scattering factors of elements are important quantities. They are a measure of how strongly and with what phase shift X-rays are elastically scattered into the diffraction pattern. For a given atom the atomic scattering factor, f, is defined as

$$^{\lambda}f = f^0 + {}^{\lambda}f' + i\,{}^{\lambda}f'' = f^0 + {}^{\lambda}\delta. \qquad (1)$$

The 'normal' amplitude is that which is appropriate for very short wavelengths. The dispersion (= wavelength dependence, always denoted by a superscript λ) of $^{\lambda}f$ is by convention described by the terms $^{\lambda}f'$ and $^{\lambda}f''$, the real and imaginary part of the 'anomalous' scattering. The f' term represents in-phase scattering and the f'' term represents scattering shifted by 90° in phase. Considering (1), the scattering from an atom located at **r** can be formally described as the sum of the scattering from two emitters at **r**: (i) an atom with scattering factor f^0 (normal scattering) and (ii) a point-like source with scattering factor $^{\lambda}\delta$. Both the magnitude and the phase of the diffracted beams can be modified to some extent merely by tuning the X-ray wavelength in the appropriate range.

Anomalous scattering can be used in different ways. In the most common way the basic structure to be determined contains many ordered atoms, *e.g.* light atoms in a protein. A few ordered atoms with detectable anomalous scattering are, or can be, inserted into the basic structure. From measurements at several wavelengths (multiwavelength anomalous dispersion or MAD) the phases of each of the measured reflections can be determined. A single crystal is sufficient, thereby ensuring strict isomorphism. The MAD method has now been successfully applied in a number of

† Now at University of Cambridge, Department of Biochemistry, Cambridge CB2 1QW, UK.

‡ Present address: Institut de Biologie Structurale, Laboratoire de Cristallographie Macromoléculaire, 41 Avenue des Martyrs, F-38027 Grenoble CEDEX 1, France.

determinations of macromolecular structures (for reviews see, for example, Fourme & Hendrickson, 1990; Hendrickson, 1991, 1994; Smith, 1991). When the anomalous scatterers are not ordered but form part of the solvent, a new method of contrast variation is unveiled (Fourme, Shepard, Kahn, l'Hermite & Li de la Sierra, 1995). This is the method of multiwavelength anomalous solvent contrast (MASC).

Sulfur is a candidate for both MAD and MASC methods. As a regular constituent in proteins it can serve as a native anomalous scatterer in protein crystallography. Sulfur in the amino acids methionine and cysteine gives rise to the X-ray absorption edge at λ = 5.02 Å (2471 eV), and that of the disulfide bridge of cystine, the dimer of cysteine, is shifted to lower energies by 1 eV (Fig. 1). These S atoms are part of a protein structure. Hence they combine biological importance with their usefulness as native labels of the MAD method. This is different with sulfur in the state of sulfate ions, as contained in many buffers used for protein crystallization. The sulfate ions are supposed to be freely moving in the solvent and it is therefore to a good approximation their wavelength-dependent contribution to the uniform electron density which defines the contrast of the protein. Moreover, the absorption edge of sulfate ions (valence +6) is at shorter wavelengths, ~5.00 Å, well separated from the region of strong dispersion due to sulfur in the valence state −2 at λ = 5.02 Å (Stuhrmann, Goerigk & Munk, 1991). This facilitates the application of the MASC method. Both cases will be treated in this paper.

The choice of trypsin as a test protein was guided by two circumstances: (i) its structure containing six disulfide bridges of cystine and two methionines is known, and (ii) its resolution is still being improved (Popov, 1996). The use of soft X-rays in protein crystallography requires another kind of instrumentation and sample environment (Stuhrmann, 1982). Some of these aspects have been presented earlier (Stuhrmann & Lehmann, 1994; Stuhrmann, Hütsch, Trame, Thomas & Stuhrmann, 1995). A more detailed discussion of the technical progress will now be given.

2. Why soft X-ray diffraction?

There is an important reason for using soft X-rays: the presence of strong anomalous dispersion from low-Z elements, such as sulfur and phosphorus, at wavelengths above 5 Å (Stuhrmann, 1982). And there is an apparently strong one against: the low penetration depth of soft X-rays in any material. 5 Å photons will propagate in air for only a few cm, and 30 μm of water is sufficient to decrease their intensity to 1/e. As a consequence of this property of soft X-rays, nearly all components of a conventional X-ray diffractometer need to be redesigned in order to make them function with soft X-rays.

Although this fact has deterred X-ray crystallographers from using soft X-rays until recently, it did not prevent them from harvesting some of the fruits of anomalous dispersion of sulfur in another way. The famous example is the determination of the structure of crambin, where the weak anomalous scattering of sulfur, remote from the K-absorption edge of sulfur, was used (Hendrickson & Teeter, 1981). This approach relied on the f''-dependent differences in the intensities of the Bijvoet pairs of each X-ray diffraction peak. The imaginary part, f'', of sulfur increases with the square of the wavelength until it reaches its maximum of ~8 e.u. (1 e.u. = 1 electron unit = scattering length of one electron = 0.28×10^{-12} cm) at the X-ray K-absorption edge at 5.02 Å. At wavelengths of 1.54 Å, which are emitted by a Cu anode of an X-ray tube, f'' of sulfur is hardly more than 0.5 e.u. Other low-Z elements show the same kind of dispersion and are likely to obscure the influence of sulfur. The striking success of the structure determination of crambin was due to the predominant contribution of the relatively numerous cystines in crambin to the Bijvoet intensity differences.

Larger differences in the intensities of Bijvoet pairs are expected at larger wavelengths (Hendrickson, 1991; Hubbard, Greenall & Woolfson, 1995). Although this improves the use of anomalous scattering with direct methods (Hubbard *et al.*, 1995), a clean separation of dispersion of different elements (and in some cases even of their chemical

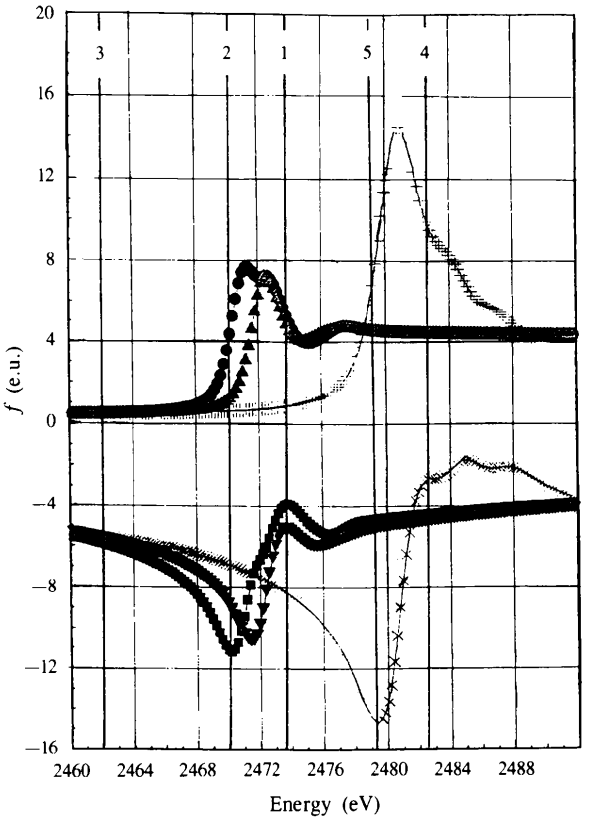

Figure 1
Anomalous dispersion of sulfur near the K-absorption edge. ▽, △ are f', f'' of methionine (cysteine); ■, ● are f', f'' of cystine; × and + are f', f'' of sulfate ions. The scattering factors are given in electron units (e.u. = scattering length per electron). The numbers inside the figure denote the indices of the chosen energies E_1–E_5.

states) can be achieved by measurements of the diffracted intensity in the near-edge region only (Fig. 1). There are two ways to proceed: either (i) the experiments are performed at wavelengths near the *K*-absorption edge of sulfur by tackling the difficult task of soft X-ray diffraction, or (ii) sulfur is substituted by its heavier homologue selenium with its *K*-absorption edge at $\lambda_K = 0.9794$ Å or even by tellurium (Boles *et al.*, 1995). There are now well established methods for the systematic biological incorporation of selenomethionine in place of methionine during protein synthesis *in vivo* (Hendrickson, Horton & LeMaster, 1990), and a number of structural studies using selenium as a substitute for sulfur have been carried out recently or are in progress (Hendrickson, 1994; Bertrand *et al.*, 1997). Alternative (i) avoids any substitution of sulfur. This was taken as an incentive for attempting the diffraction of 5 Å photons from single crystals of lysozyme (Lehmann, Müller & Stuhrmann, 1993). Only 20 X-ray diffraction spots could be collected at that time. Since then, technical progress has very much improved the conditions of soft X-ray diffraction experiments and the number of reflections collected from a single crystal of a protein has been increased by two orders of magnitude. Recent results of diffraction experiments from single crystals of trypsin are presented as a reference of the method.

3. The technique of soft X-ray diffraction

A diffractometer for soft X-ray diffraction as shown in Fig. 2 was first developed at HASYLAB, Hamburg (Stuhrmann *et al.*, 1991), and a very much improved version is presently under construction at the ESRF, Grenoble. The design is guided by the minimization of X-ray absorption. As mentioned above, the penetration depth of 5 Å photons in air is ~3 cm and only ~30 μm in biological matter and polymers, which in this respect may well be represented by water. This means that the beam path should be evacuated and windows, if unavoidable, should be thin. Diffraction from a protein crystal will emerge from regions defined by the low penetration depth which may be only a small fraction of the crystal size. Backscattering is favourable. Fortunately, this is what prevails with soft X-ray diffraction. Diffraction peaks corresponding to a structural resolution from 3.5 to 2.5 Å are observed at angles between 90° and extreme back reflection at 180° when 5 Å photons are used.

Moreover, the average intensity of diffracted beams is proportional to λ^2 (Harding, 1996), which to a good extent compensates for the influence of the absorption coefficient increasing with λ^3. A reasonably high diffraction intensity is expected with soft X-rays provided the design of the diffractometer copes with the conditions mentioned above.

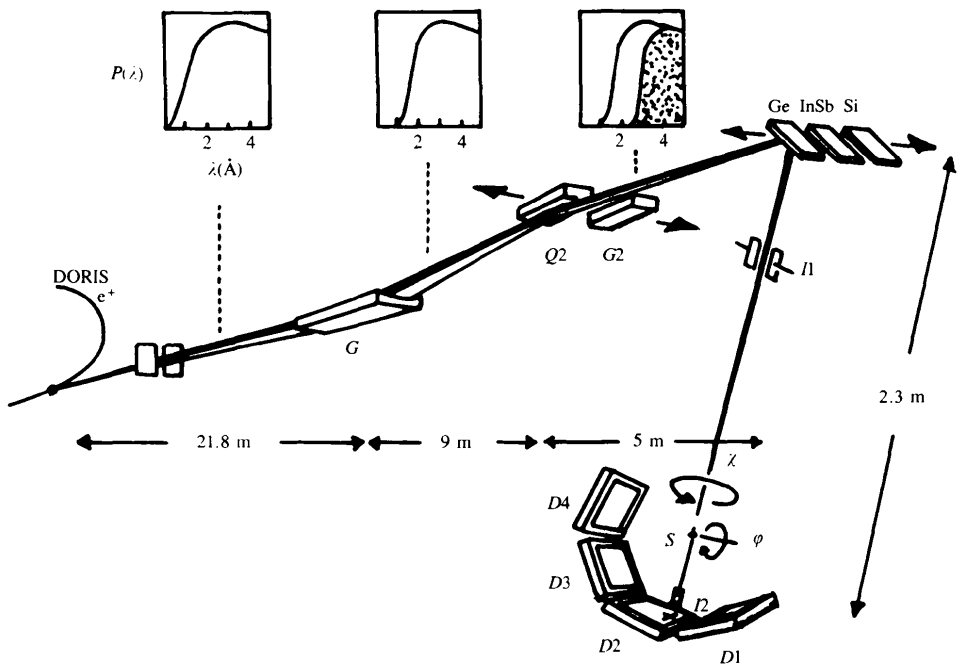

Figure 2
The X-ray diffractometer at beamline A1 of HASYLAB (until December 1996). Synchrotron radiation from the storage ring DORIS is focused by the Au-coated toroidal mirror (*G*), the mean angle of vertical deflection being 14 mrad. A second flat mirror has two surfaces, an Au-coated one (*G*2) and that of the naked quartz substrate (*Q*2). Either surface can be moved into the beam, resulting in different transmitted spectra $P(\lambda)$ shown in the insert. There are three crystal monochromators resident in the evacuated monochromator housing. The ionization chambers *I*1 and *I*2 are used for measurement of the X-ray absorption by the sample and for control of the wavelength. The diffraction pattern of the sample (*S*), recorded by four area counters *D*1, *D*2, *D*3 and *D*4, is stored in fast memory units which are read out by a VAX 11/45 computer after periods of several minutes. There is no window between the storage ring and the ionization chamber *I*1.

3.1. *X-ray detectors and windows*

One immediate consequence of the use of long wavelengths is that the diffractometer should have a detector system accepting the diffracted intensity in a wide angular range. This requirement is met with the instrument at beamline A1 of HASYLAB by putting four area counters on a circle of 0.55 m radius around the sample (Fig. 3). Each of these multiwire proportional counters (MWPC) has a sensitive area of 300 × 300 mm^2, in total covering 10% of 4π. The extremes of the scattering angles reached by this arrangement are $2\theta = -50$ and $+120°$.

The area detectors have been developed at the EMBL Outstation at Grenoble and further improved at GKSS, Geesthacht. The usual specifications of the wire planes (Au-coated W wires of 6 μm thickness for the anode) are convenient for soft X-ray diffraction. A mixture of argon/ethane (7:1) is very efficient for the detection of soft X-rays. As the electric pulses created by low-energy X-ray photons are relatively small, a careful discrimination against noise is important.

Large windows of 300 × 300 mm^2 separate the gas-filled MWPCs from the evacuated housing of the two-circle goniometer. Each window is a system of layers which in total combines mechanical stability and vacuum tightness with high transparency for soft X-rays (Scholl *et al.*, 1995). Recent experience has shown that Kevlar nets (60 g m^{-2}) tend to show signs of fatigue after many pumping cycles. The presently used windows with a transparency of 0.3 for 5 Å photons consist of a steel grid of 3 mm mesh size and 0.25 mm wire thickness as a mechanical support and three polypropylene foils of 4 μm thickness on the steel grid, sufficient to maintain a pressure of less than 5 × 10^{-3} mbar in the goniometer housing. A Kapton foil of 7 μm thickness separates the detector gas from the helium buffer volume.

Another absorber is the ionization chamber (*I*1 in Fig. 2) just behind the monochromator, which serves as a flux monitor. It is filled with air at a pressure of 50 mbar (like *I*2) and has a depth of 5 cm. The plastic windows on both sides of chamber *I*1 have a thickness of 10 μm each.

A differential pumping system which has been installed by HASYLAB gives windowless access to the DORIS storage ring, *i.e.* there are no windows between the first ionization chamber *I*1 and the source. To avoid any conflict with the high vacuum of the storage ring the pressure inside the goniometer housing has to be kept below 0.01 mbar.

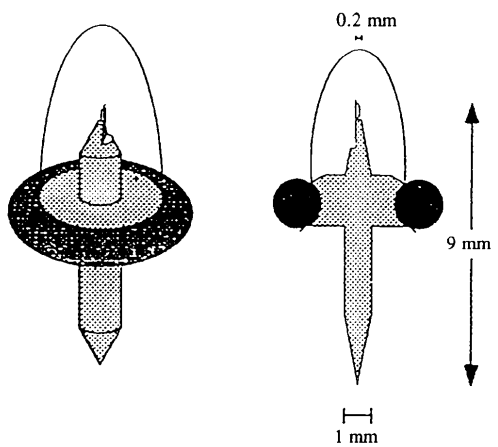

Figure 3
The sample cell is a titanium needle of length 9 mm, carrying on its tip the protein crystal. An *O*-ring fixes a thin-walled plastic dome. The assembly is described in Fig. 4.

3.2. *X-ray optics and focusing capillary*

The X-ray optics used for focusing and monochromatization consists of two mirrors and one crystal monochromator, all beam deflections being in the vertical plane because of the predominantly horizontal polarization of synchrotron radiation (Stuhrmann *et al.*, 1991). The integrated intensity of the focal spot of ~10 mm^2 is 10^{10} photons s^{-1} at $\lambda = 5$ Å. This is a very large cross section of the beam compared with that of a protein crystal. Attempts have therefore been made to concentrate the photon flux on the protein crystal using a focusing glass capillary of 0.7 m length in front of the sample. The capillary presently in use has a convergent inner cross section close to that of a parabola (Stuhrmann, Bartels *et al.*, 1996). The diameters at the entrance and the exit of the capillary are 1.8 and 0.8 mm, respectively. It ends at 2 cm in front of the sample cell. There is a gain in flux at the sample by a factor of five at the cost of a slightly increased divergence of the emerging beam. This is what is expected from a capillary concentrator (Bilderback, Thiel, Pahl & Brister, 1994; Balaic, Nugent, Barnea, Garrett & Wilkins, 1995; Engström & Riekel, 1996).

3.3. *Sample environment*

The two-circle goniometer with the sample is in an evacuated environment (Scholl *et al.*, 1995). This defines both the mounting procedure of the protein crystal and the protection of the crystal from drying. Moreover, it is necessary to reduce radiation damage by cooling.

In a first step it was ensured that the protein crystal was kept in a humid atmosphere. A vacuum-tight sample cell with a volume close to that of a thumb was used for the first measurement of soft X-ray diffraction from tetragonal lysozyme at room temperature (Lehmann *et al.*, 1993). The fairly large sample cell used in the early experiment was replaced by smaller and smaller cells with increasingly large opening angles for the diffracted intensity. The final result of this development is shown in Fig. 3.

The miniaturization of the sample cell also facilitated the implementation of a cooling system. Peltier cascades were preferred because of their small size and because they are easy to operate. The basic temperature of the device with five stages, from AMS Thermotech (Munich), was 158 K when the warmer side of the cascade was kept at 248 K.

The crystal is mounted in the following way. A small plastic foil (hostaphan, 8 μm) is glued to the tip of a titanium needle (Fig. 3). This device is used to fish a protein crystal in the cryoprotective solution (see below) held in a watch glass under a microscope. Any residual mother liquor

adhering to the crystals is removed by a filter tip. The titanium needle with the crystal is placed onto a liquid-nitrogen-cooled brass block inside a styrofoam box (Fig. 4). The atmosphere of cold nitrogen gas inside this box freezes the crystal to ~213 K within a few seconds. Then the upper part of the needle with the protein crystal is rapidly closed with a plastic dome which is held by an *O*-ring. The mechanical precision and speed is ensured by a special device shown in Fig. 4. The box with the cooled crystal inside is brought as close as possible to the goniometer head with the Peltier cascade. With a special pair of pliers the titanium needle is taken out of the box and inserted into the borehole of a small brass plate on top of the cold Peltier cascade. The atmosphere inside the open vacuum vessel must remain very dry in order to avoid ice formation. This is achieved by flushing the vessel with dry nitrogen gas while the crystal is being mounted. Then the nitrogen stream is cut, the vessel is closed immediately thereafter and evacuated to a pressure of some 10^{-3} mbar within 10 min.

3.4. *Multiwire proportional counters versus imaging plates*

The requirement to measure the diffracted intensity over a wide range of scattering angles simultaneously is met most easily by imaging plates. They are flexible and can be bent to form a cylinder around the diffracting crystal allowing for simultaneous measurement of the diffracted intensity from small angles near the beam stop to large angles close to the direction opposite to that of the incident beam. An arrangement of several multiwire proportional counters (MWPCs) on a circle, as shown in Fig. 2, is less efficient as there are gaps between the sensitive areas of adjacent detectors.

Image plates are as sensitive to soft X-rays as MWPCs are. In a test experiment the diffraction of 5 Å photons from a trypsin crystal was observed simultaneously with a MWPC (*D*3 in Fig. 2) and with an imaging plate shadowing the detector *D*1. The result was that the number of events recorded in the diffracted peaks was almost the same for both types of detectors. However, the spots on the imaging plates were sharper and the background was somewhat smoother and higher than on the MWPC (see *e.g.* Lewis, 1994).

This test shows that imaging plates are the most powerful detectors in soft X-ray diffraction as they combine high sensitivity with the simultaneous measurement of the diffracted intensity over a wide angular range, provided the readout system is adapted to cylindrically bent plates used in an evacuated environment. No similar problems exist with MWPCs, where the storage of each event occurs by direct memory access.

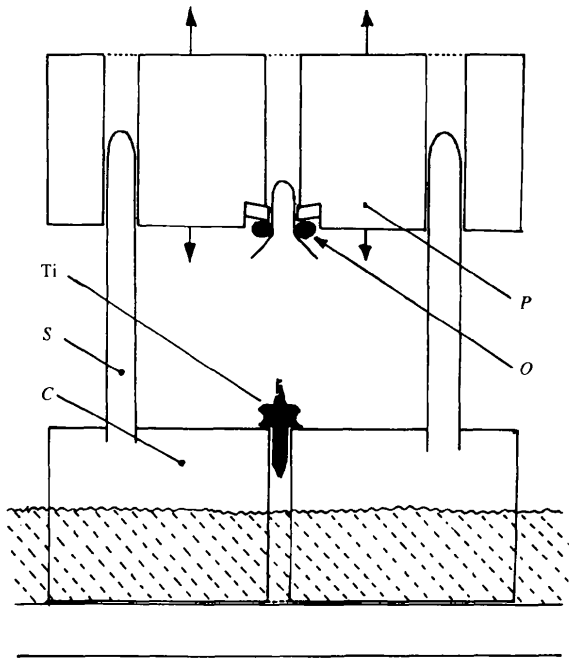

Figure 4
The sample cell with its mounting device. The titanium needle (Ti) with the protein crystal on top is placed onto a liquid-nitrogen-cooled brass block (*C*). The plastic cap with the *O*-ring, fixed to a plastic block (*P*) by a drop of grease, is pushed downwards while being guided by two steel rods (*S*).

4. Crystallization of bovine trypsin

Purified bovine trypsin was crystallized from a buffer containing 2.5 *M* ammonium sulfate, 1 *M* benzamidine (inhibitor), 10 *M* $CaCl_2$ and 10 *M* morpholinoethane sulfonic acid. Under these conditions crystals were obtained in the form of needles with unit-cell dimensions a = 54.9, b = 58.4, c = 67.7 Å and the orthorhombic space group $P2_12_12_1$, the same as published by Bode & Huber (1978). These crystals were soaked for 10 min in a cryoprotectant solution which contained the original buffer adjusted to pH 5 with an excess of synthetic sugar, Phytohistol (80%) and ethylene glycol (10%), and mounted according to the procedure described above.

5. Data collection

Diffraction data were collected from 15 crystals at three wavelengths (see below) near the *K*-absorption edge of sulfur as it is characteristic for methionine and the disulfide bridges of cystine (Fig. 1). A set of ten contiguous 1° oscillation exposures were taken at each of the chosen wavelengths in turn, then continuing with the next 10° in φ with one exposure overlap. The exposure time varied from 2 to 4 min per 1° depending on the current of the storage ring DORIS. It therefore took slightly more than 1 h to measure the dispersion over a rotation angle of 10°. Ideally, a scan over 180° could have been finished in less than 1 d. In practice, twice that time was needed, owing to breaks in the operation of the storage ring and changes of the beam position which required a new calibration of the wavelength scale. Only two of the 15 crystals kept diffracting for 2 d. Another five allowed a scan of not more than 60° each. Some had to be discontinued due to mechanical or

electronic problems of the instrument or they did not diffract reasonably well.

The trypsin crystals diffracted to the maximum scattering angle of 120° as defined by the instrument corresponding to a structural resolution of 2.9 Å. Fig. 5 shows the distribution of the diffraction peaks on the four area counters after a 1° oscillation. There are, of course, many fewer peaks visible than one usually observes on a still taken at wavelengths of ~1 Å.

6. Choice of the wavelengths

The intensity of the diffraction peaks was measured at three wavelengths near the *K*-absorption edge of sulfur in cystine. The wavelengths have been chosen in such a way that the triangle connecting the (f_i', f_i'') coordinates of sulfur in the plane of complex numbers at wavelengths λ_i (i = 1, 2, 3) is almost equilateral. In this way the edges of the triangle represent reasonably well the anomalous dispersion of sulfur (Fig. 6). Two of them (i = 1, 2) have almost equal values of f'' and the intensities observed at these wavelengths are therefore equally attenuated. The third wavelength was chosen at the low-energy side of the absorption edge. This is shown for the structure factor F_{293} of trypsin. This strategy has some obvious advantages, such as the relatively easy correction for absorption, but it ignores the role of the f''-dependent Bijvoet pairs.

The dispersion of F_{293} shown in Fig. 6 is slightly different from that of $F_{\bar{2}9\bar{3}}$. This is because S atoms in two different states, S in methionine and S of the disulfide bridges of cystine, contribute to anomalous dispersion. There is also a shift and a small inclination of the dispersion figure due to the dispersion of the real part f' of the sulfate ions. These effects will become important in more detailed studies. They are neglected here.

The dispersion of the sulfate ions is well separated from that of sulfur in the valence state (−2). The wavelengths λ_4

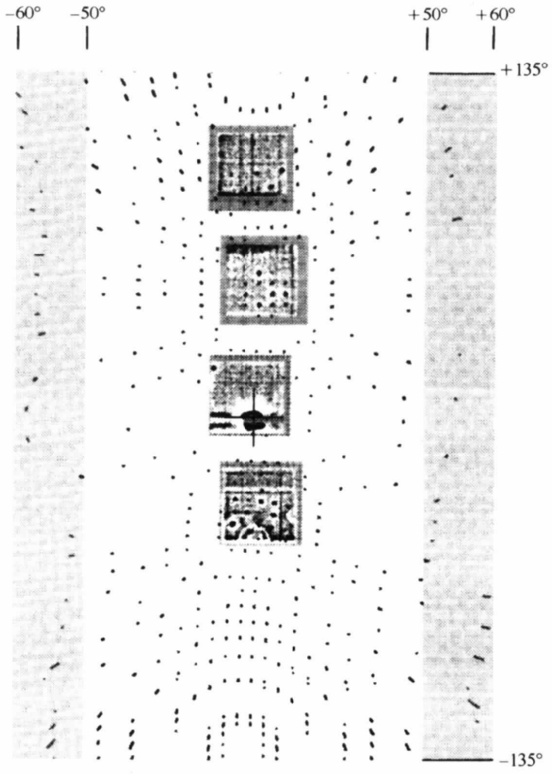

Figure 5
Diffraction of 5 Å photons by trypsin as collected by the four area counters shown in Fig. 2. The detectors are arranged on a vertical circle of 1.1 m diameter around the sample in the centre. They cover scattering angles from −60 to +120° (close to the top of the figure). The beam stop is marked by a cross. Although each of the densely spaced detectors has a sensitive area of 30 × 30 cm^2, the solid angle which they cover is only 10% of the unit sphere. A very much increased solid angle could be accessed by a cylindrical bent imaging plate, which may accept angles of diffraction from −135 to +135° in the azimuth of the cylinder and polar angles of diffraction from −60 to +60° if the shaded area is included. This is two-thirds of the unit sphere. The solid angle is slightly reduced with the polar angles of ±50° shown by the blank area. The diffraction spots outside the used sensitive area of the detectors have been calculated on the basis of the known indices (*hkl*) of the measured Bragg reflections from trypsin. The trypsin crystal has been rotated by 1° around the axis of the cylinder.

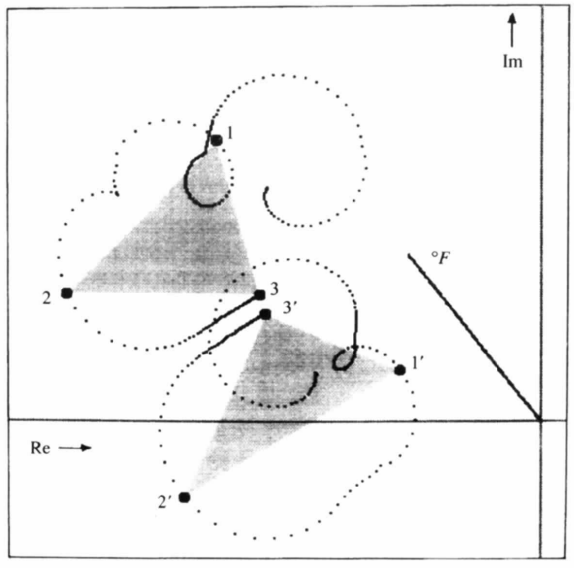

Figure 6
The dispersion of the structure factors F_{293} and $F_{\bar{2}9\bar{3}}$ of trypsin near the *K*-absorption edge of sulfur. The dispersion of both F shows two almost closed contour lines. The smaller almost spherical contour line is due to the sulfate ions (valence state +6) whereas the larger less-spherical contour line is due to sulfur in the valence state −2. It is only the latter which varies slightly in shape when passing from F_{293} to $F_{\bar{2}9\bar{3}}$. This is due to the contribution of two types of S atoms, *i.e.* those of the six disulfide bridges and of the two methionines. The wavelengths at which the anomalous diffraction has been measured are marked by large dots. They were chosen in such a way that they form a triangle of almost maximum area (shaded). The reflection has been taken as an example because of its relatively strong dispersion and its unusually small $^\circ F$. The structure factors obtained from measurements at three different wavelengths (1, 2, 3 for $|^{\lambda i}F_{293}|$ and 1′, 2′, 3′ for $|^{\lambda i}F_{\bar{2}9\bar{3}}|$) agree with the calculated values within an error of about 20% of $^\circ F$.

electronic problems of the instrument or they did not diffract reasonably well.

The trypsin crystals diffracted to the maximum scattering angle of 120° as defined by the instrument corresponding to a structural resolution of 2.9 Å. Fig. 5 shows the distribution of the diffraction peaks on the four area counters after a 1° oscillation. There are, of course, many fewer peaks visible than one usually observes on a still taken at wavelengths of ~1 Å.

6. Choice of the wavelengths

The intensity of the diffraction peaks was measured at three wavelengths near the *K*-absorption edge of sulfur in cystine. The wavelengths have been chosen in such a way that the triangle connecting the (f_i', f_i'') coordinates of sulfur in the plane of complex numbers at wavelengths λ_i (i = 1, 2, 3) is almost equilateral. In this way the edges of the triangle represent reasonably well the anomalous dispersion of sulfur (Fig. 6). Two of them (i = 1, 2) have almost equal values of f'' and the intensities observed at these wavelengths are therefore equally attenuated. The third wavelength was chosen at the low-energy side of the absorption edge. This is shown for the structure factor F_{293} of trypsin. This strategy has some obvious advantages, such as the relatively easy correction for absorption, but it ignores the role of the f''-dependent Bijvoet pairs.

The dispersion of F_{293} shown in Fig. 6 is slightly different from that of $F_{\bar{2}9\bar{3}}$. This is because S atoms in two different states, S in methionine and S of the disulfide bridges of cystine, contribute to anomalous dispersion. There is also a shift and a small inclination of the dispersion figure due to the dispersion of the real part f' of the sulfate ions. These effects will become important in more detailed studies. They are neglected here.

The dispersion of the sulfate ions is well separated from that of sulfur in the valence state (−2). The wavelengths λ_4

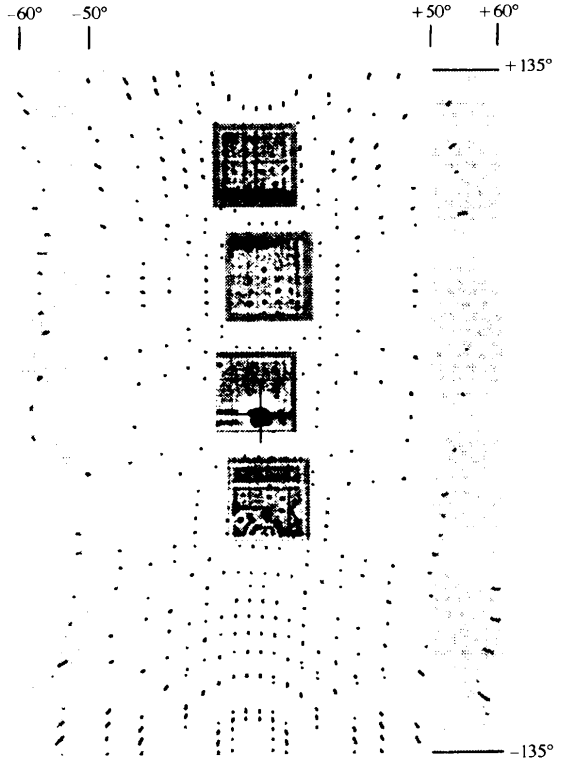

Figure 5
Diffraction of 5 Å photons by trypsin as collected by the four area counters shown in Fig. 2. The detectors are arranged on a vertical circle of 1.1 m diameter around the sample in the centre. They cover scattering angles from −60 to +120° (close to the top of the figure). The beam stop is marked by a cross. Although each of the densely spaced detectors has a sensitive area of 30 × 30 cm^2, the solid angle which they cover is only 10% of the unit sphere. A very much increased solid angle could be accessed by a cylindrical bent imaging plate, which may accept angles of diffraction from −135 to +135° in the azimuth of the cylinder and polar angles of diffraction from −60 to +60° if the shaded area is included. This is two-thirds of the unit sphere. The solid angle is slightly reduced with the polar angles of ±50° shown by the blank area. The diffraction spots outside the used sensitive area of the detectors have been calculated on the basis of the known indices (*hkl*) of the measured Bragg reflections from trypsin. The trypsin crystal has been rotated by 1° around the axis of the cylinder.

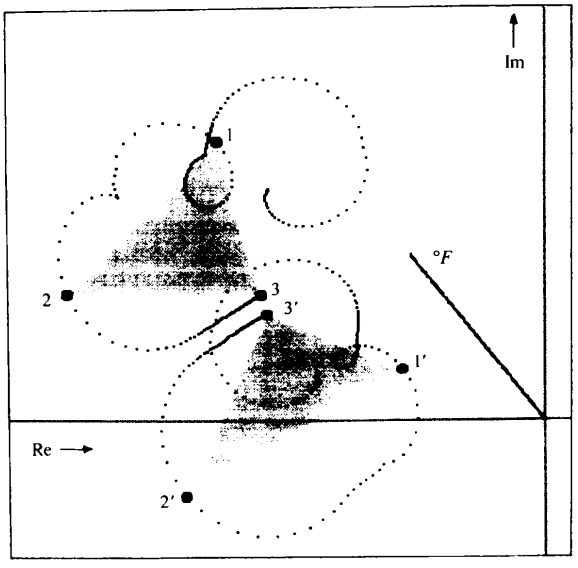

Figure 6
The dispersion of the structure factors F_{293} and $F_{\bar{2}9\bar{3}}$ of trypsin near the *K*-absorption edge of sulfur. The dispersion of both F shows two almost closed contour lines. The smaller almost spherical contour line is due to the sulfate ions (valence state +6) whereas the larger less-spherical contour line is due to sulfur in the valence state −2. It is only the latter which varies slightly in shape when passing from F_{293} to $F_{\bar{2}9\bar{3}}$. This is due to the contribution of two types of S atoms, *i.e.* those of the six disulfide bridges and of the two methionines. The wavelengths at which the anomalous diffraction has been measured are marked by large dots. They were chosen in such a way that they form a triangle of almost maximum area (shaded). The reflection has been taken as an example because of its relatively strong dispersion and its unusually small °F. The structure factors obtained from measurements at three different wavelengths (1, 2, 3 for $|^{\lambda i}F_{293}|$ and 1′, 2′, 3′ for $|^{\lambda i}F_{\bar{2}9\bar{3}}|$) agree with the calculated values within an error of about 20% of °F.

is a sharp decrease in the completeness to zero at $4 < d < 3.4$ Å, which is due to the gap between the area detectors $D3$ and $D4$ in Fig. 2. The reflections recorded by the area detector $D4$ give rise to an increase of the completeness to 0.4 at $3.4 < d < 2.9$ Å. This is what would be observed with all reflections strong enough to be recorded by the four detectors; in other words these are the measured (hkl). Looking into the intensities $I(hkl)$, the situation hardly changes at low structural resolution ($d \geq 5$ Å). Almost all predicted reflections exhibit an intensity higher than 3σ and the intensity of two-thirds of them exceeds 5σ. At higher resolution ($3.4 < d < 2.9$ Å) the fraction of measured $I(hkl)$ with $I/\sigma \geq 3$ is 15% and drops to 5% for $I/\sigma \geq 5$.

There are two reasons for this behaviour: (i) the reflections at larger angles always tend to be weaker, and (ii) there is a decay of the scattering intensity with time which increases with the length, $s = 1/d$, of the scattering vector.

The latter point is crucial in soft X-ray diffraction and will be discussed in more detail.

7.2. *Radiation damage*

The decrease of the intensity diffracted by single crystals of trypsin with time and the scattering angle is shown in Fig. 8. It is slow, with reflections corresponding to low structural resolution ($d > 5$ Å), the half-time being ~10 h. The decay of the intensity is three times faster with reflections corresponding to higher structural resolution $d < 4$ Å. These decay times refer to a set of ten contiguous 1° oscillation exposures taken at three wavelengths, typically within a time of slightly more than 1 h at the beginning of the experiment. Estimates of radiation damage from irradiation by soft X-rays have been given recently for electron microscopy (Henderson, 1995) and for diffraction from protein crystals (Polikarpov, 1997).

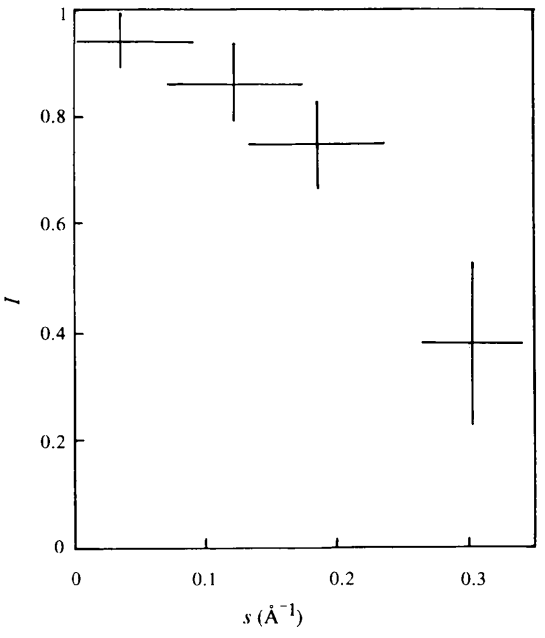

Figure 8
The decrease of the intensity of 5 Å photons diffracted by trypsin crystals within 1 h. The average is taken over each detector separately. The horizontal lines describe their ranges in $s = 1/d$. The vertical lines indicate the spread of the decay times found with different crystals.

While the crystal is rotated, fresh parts of the protein crystal become exposed to the incident beam. This is the reason why reflections at large s ($s = 1/d > 0.2$ Å^{-1}) are observed even after one day of continuous data collection. A medium-sized protein crystal (0.3 mm) absorbs the incident beam of soft X-rays very efficiently, thus protecting the crystal surface not yet exposed to the beam. This is different from diffraction of deeply penetrating high-energy X-rays where fresh parts of a crystal are found by a small displacement of the sample with respect to the incident beam.

The experiments confirm an increased radiation damage of protein crystals when irradiated by low-energy X-ray photons, although to an extent which is smaller than that predicted by Polikarpov (1997). Following an argument of Henderson (1995), which states that the amount of damage (energy deposited) per useful event (elastic scattering) should be relatively independent of the energy of the incident X-ray beam, the increased sensitivity of protein crystals to soft X-rays is explained by the fact that the photon energy is essentially deposited onto the crystal surface rather than in the volume of a normal-sized protein crystal.

8. Dispersion of sulfur in trypsin

When the local scaling procedure defined by (2) is applied to the anomalous-diffraction data from the various trypsin crystals, the deviation of the measured data from the corresponding calculated values yields an R value (in terms of $|F|$) of 0.13. Taking into account a resolution-dependent degradation of the crystal with time by exponential decay functions, the R value drops to 0.10.

It has been observed during the experiments that the beam position changed and so did the wavelength transmitted by the monochromator. After a correction for this the R value decreased to 0.09 (in terms of $|F|$).

The mean expected variation of the intensity (Crick & Magdoff, 1956) due to the anomalous dispersion of the six disulfide bridges of cystine and two methionine S atoms of trypsin (M = 23.8 kD) is 0.2 (or 0.1 in terms of $|F|$), dispersion of absorption excepted. The change of the intensity due to the f''-dependent dispersion penetration depth results in an additional variation of the intensity of the same amount of 0.2.

The dispersion of the diffracted intensity is

$$|^{\lambda}F(\pm\mathbf{h})|^2 = |U(\mathbf{h})|^2 + a(\lambda)|V(\mathbf{h})|^2 + b(\lambda)|U(\mathbf{h})||V(\mathbf{h})|\cos(\Delta\varphi) \pm c(\lambda)|U(\mathbf{h})||V(\mathbf{h})|\sin(\Delta\varphi), \quad (3)$$

where $a(\lambda) = {}^{\lambda}f'^2 + {}^{\lambda}f''^2$, $b(\lambda) = 2({}^{\lambda}f')$ and $c(\lambda) = 2({}^{\lambda}f'')$ and $\Delta\varphi$ is the phase difference $(\varphi_U - \varphi_V)$. $U(\mathbf{h})$ is the structure factor of all atoms off resonance and $V(\mathbf{h})$ is the structure factor of atoms with strong anomalous dispersion at a reciprocal lattice vector $\mathbf{h}$. Dispersion analysis according to (3) implies a two-step process for the phasing procedure: (i) find the atomic coordinates of the anomalous scatterers [either by direct methods, using $|V(\mathbf{h})|$ resulting from this analysis, or from some kind of difference Patterson map]; (ii) exploit the $\Delta\varphi$ term of the dispersion formula for the eventual phase calculation of $U(\mathbf{h})$.

9. Localization of the S atoms

There are $4 \times 14 = 56$ S atoms per unit cell, giving rise to a rather complex Patterson map consisting of $(56 \times 55)/2 = 1540$ peaks. Out of the 56 S atoms there are 4×6 disulfides, which not only outnumber the isolated 4×2 methionine S atoms but at low Bragg resolution are not resolved and are therefore expected to dominate the picture. Even a reduced set of disulfides together with the methionines would give rise to $(32 \times 31)/2 = 496$ distinct difference vectors, at least $(6 + 2) \times 4$ on each Harker section. Not to mention the influence of the resolution of 5 Å which will lead to serious overlaps and give additional features to the Harker section. Patterson maps of that complexity are difficult to analyze. Hence, the determination of sulfur coordinates will have to rely on direct methods. For this purpose a reasonable number (some hundred, see below) of $|V_{hkl}|$ needs to be determined from triples of $|{}^{\lambda}F_{hkl}|$. An approximate expression for $|V|$ is given by half the sum of the differences $|F(\lambda_1) - F(\lambda_2)|$, $|F(\lambda_2) - F(\lambda_3)|$, $|F(\lambda_3) - F(\lambda_1)|$, where $F(\lambda_i)$ denotes $|{}^{\lambda i}F_{hkl}|$. This is a lower estimate of $|V|$. It is corrected by fitting the edges of the appropriately scaled and rotated triangle (Fig. 6) representing the dispersion of f' and f'' of sulfur to the experimental $|{}^{\lambda i}F_{hkl}|$. The correction factor varies between 1.0 and 1.2 with this description of the dispersion.

Although the completeness of the data is close to 80% at 5 Å resolution and 30% in the resolution shell from 3.4 to 2.9 Å, only slightly more than half of the integrated peak intensities ($I > 4\sigma$) were considered to be suitable for further analysis; also a rejection ratio of $|\Delta I_{ano}|/I < 2$ corresponds to the expected maximum change. Moreover, the reflections at $s = 1/d \geq 0.2$ Å^{-1} were discarded. Hence, 460 reflections were left for the calculation of the coordinates of the S atoms by the program *SHELXS*86 (Sheldrick, 1990).

Before entering into the analysis of the experimental data, a series of tests were performed using the known model of trypsin [Marquardt *et al.*, 1983 (PDB reference 1TPO); Popov, 1996]. The resolution limit was varied between 2.5 and 10 Å. It turns out that the positions of the S atoms (disulfide bridges are considered as a single scattering centre) can be deduced unambiguously from anomalous-diffraction data even at a structural resolution of 4 Å. All the six disulfide bridges and the S atoms of the two methionines of the asymmetric unit have been found by *SHELXS*86. For the hypothetical case of diffraction of S atoms alone, *SHELXS*86 finds the correct coordinates even at a resolution of 6 Å.

Table 1
Comparison of the sites of S atoms of trypsin localized by *SHELXS*86 with those of the known model of trypsin.

Number	Scattering centres of sulfur†	Deviation (Å) from expected position (y, z)
1	Cys1–Cys6	1.6
2	Cys9–Cys11	2.7
3	Cys5–Cys10	1.6
4	Cys4–Cys12	1.2
5	Cys2–Cys3	6.5
6	Met1	3.9
7	Met2	14.4
8	Cys7–Cys8	17.2

† Cys = cystine, Met = methionine.

In practice, experimental data are noisy and incomplete. The 460 structure factors $|V_{hkl}|$ of trypsin deduced from anomalous dispersion near the K-absorption edge of sulfur are limited in resolution and completeness as mentioned above. Moreover, the trypsin crystals were rotated around an axis close to (h00) resulting in a lower completeness in that direction. It is therefore not surprising that the x coordinates remained undefined, and the coordinates in the yz plane of five out of eight scattering centres of sulfur were identified by *SHELXS*86 within deviations of less than 4 Å from the known coordinates (Table 1). The first six scattering centres exhibit a mean deviation of 2.9 Å from the known positions.

The agreement of the 460 structure factors $|V_{hkl}|$ with those calculated from the known trypsin model is given by $R = 0.48$. The Patterson map based on these reflections correlates with that calculated from the model at 5 Å resolution as described by the normalized correlation coefficient (*CCP4*; SERC Daresbury Laboratory, 1993) of 0.60 (Fig. 9).

10. Phasing Bragg reflections

In the calculation of the Fourier map the dispersion of 775 unique reflections (+183 Bijvoet pairs) was taken into account. This number is slightly higher compared with that used for the localization of the S atoms as the upper limit of $s = 1/d$ was increased from 0.2 to 0.35 Å^{-1}.

The procedure of phasing Bragg reflections emerges from the method used to determine $|V_{hkl}|$. The additional feature is that V_{hkl} is known both in amplitude and in phase, because the positions of the S atoms have been determined. The edges of the triangle described by ${}^{\lambda i}V_{hkl}$ (Fig. 6) will have to be displaced (at constant orientation) in such a way that they come close to the triplet of experimental $|{}^{\lambda i}F_{hkl}|$ as shown in Fig. 6. This procedure has been tested and used for the determination of phases of U_{hkl}. It is easily extended to the case of more than three wavelengths. A more elaborate

procedure which has not yet been used here is offered by the treatment of the MAD data as a case of multiple isomorphous replacement, *e.g.* in *MLPHARE* (maximum likelihood phase refinement) (Otwinowski, 1993).

In the following discussion the approximate sites of the S atoms, which have been derived from the experimental data by *SHELXS*86, will be replaced by those of the known model.

The result of the phasing and subsequent Fourier synthesis is the electron density map of trypsin shown in Fig. 10 (shaded). The map correlates with that deduced from the known model of trypsin (contour lines in Fig. 10) at 5 Å resolution as described by the normalized correlation coefficient of 0.52. The mean deviation of the phases determined from the dispersion of the diffraction intensity from those calculated from the trypsin model is 65°. The scatter, $\delta\varphi$, of evaluated phases from symmetric equivalent phases is 45° with respect to their mean value (Stuhrmann *et al.*, 1997).

11. Looking for anisotropic anomalous scattering

When the excited state lacks high symmetry and is oriented in the crystal by chemical bonding, the resonance or anomalous dispersion is dependent on the polarization geometry and the anomalous scattering can no longer be represented as a scalar.

The X-ray absorption edge of sulfur in cystine shows two peaks separated by slightly more than 1 eV (Fig. 1). While it has one of them in common with both cysteine and methionine, the other peak on the low-energy side at 2470 eV is typical of the disulfide bridge of cystine. It is assumed that the photoelectric interaction of X-rays giving rise to this peak and the X-ray emission is dependent on the orientation of the disulfide bond (Fig. 11). The derivation of the experimental evidence from the diffraction data will therefore be attempted. There is also anisotropic anomalous scattering from sulfur in methionine (Fanchon & Hendrickson, 1990) which is not considered here.

The orthorhombic symmetry of the trypsin unit cell is a favourable condition for anisotropic anomalous scattering. Moreover, the distribution of the direction of the disulfide bonds inside the four trypsin molecules of the unit cell is highly anisotropic. The sum of the squares of the projections is 0.527, 0.096 and 0.370 in the x, y and z directions, respectively. Following the theory developed by Templeton & Templeton (1980) and as has been shown by the pioneering experiments of the same authors (*e.g.* Templeton & Templeton, 1985), any directional property of the anomalous-scattering process related to sulfur, and in particular to the disulfide bonds of cystine, should become measurable.

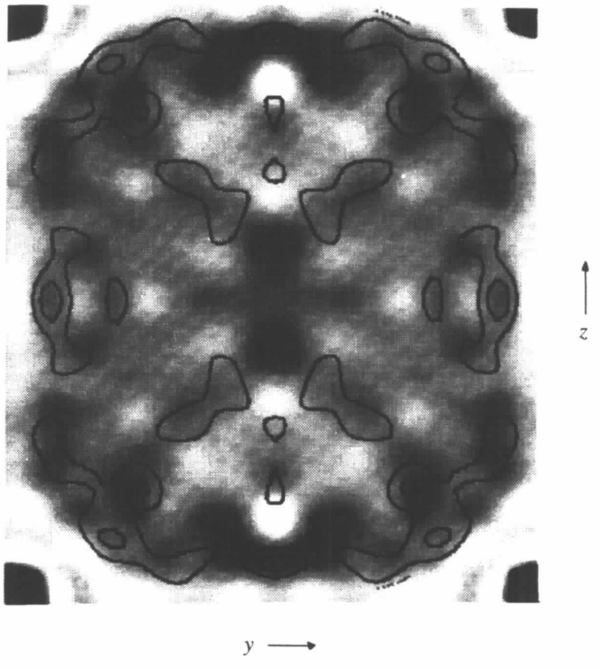

Figure 9
Difference Patterson maps of sulfur in trypsin. They were calculated on the basis of the following differences of the structure factors: $|F(\lambda_1)| - |F(\lambda_2)|$, $|F(\lambda_2) - F(\lambda_3)|$ and $|F(\lambda_3) - F(\lambda_1)|$. The experimental data (shaded) are compared with those obtained from the model (contour lines) at 5 Å resolution. The yz plane of the Patterson map is shown at $x = 0$.

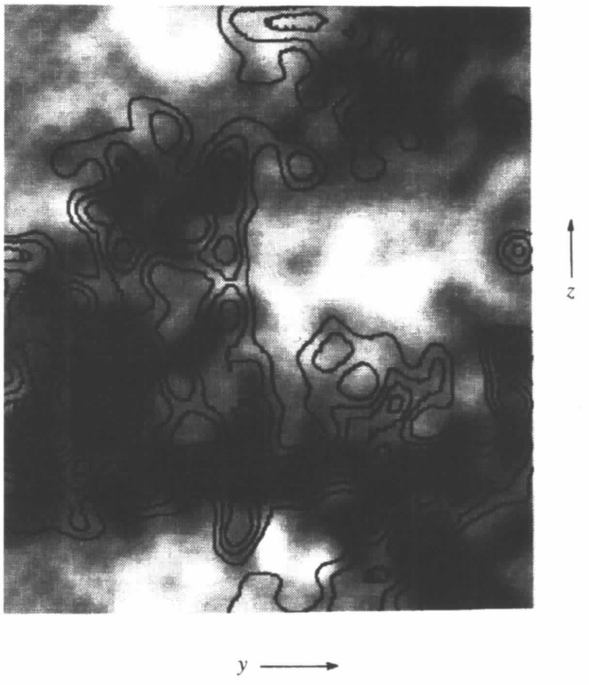

Figure 10
Fourier synthesis from 775 unique reflections of trypsin. The reflections have been phased by using intensity data measured at wavelengths λ_1, λ_2, λ_3, and the known coordinates of the S atoms in the orthorhombic unit cell. The electron density in the yz plane at $0.75 < x < 0.85$ is shown in grey. The electron density map of the known trypsin model (Popov, 1996) is presented by contour lines. Both maps are limited to 5 Å resolution.

The data analysis makes use of the following model: the difference between the absorption spectrum of cysteine and that of cystine be associated with the interaction of the X-rays with the disulfide bridges (Fig. 1). It is represented by a Gaussian fitted to the peak which has been assigned to the disulfide bridge. Moreover, it is assumed that the difference spectrum should develop fully when the electrical vector of the incident radiation is parallel to the S—S bond direction and if the direction of the diffracted beam is orthogonal to the disulfide bond. The polarization of the monochromated X-ray synchrotron radiation is regarded as linear (Fig. 11). The intensity emitted by each disulfide bridge is described by $a + b\cos^2\gamma$, where γ is the angle between the line connecting the S atoms of a disulfide bridge and the direction of the diffracted beam. A necessary condition for the validity of the model is that the coefficient b be negative.

Starting from these assumptions and introducing a and b as additional variables, the R value from the comparison of measured amplitudes with those calculated from the model has been further decreased by about 0.5%. This could probably not be taken as a sufficient argument as any other additional parameter might work similarly, independent of its physical relevance. More convincing is the result obtained from a separate analysis of each crystal. The coefficient b does turn out to be negative in all cases. An anisotropy of anomalous scattering develops to a degree of 0.07 ± 0.07 of the maximum possible value defined by the model of f''. This is an indication that the orthorhombic form of trypsin does give rise to anisotropic anomalous scattering in the frame of the model. The intensities of the 'forbidden' reflections ($h00$: $h = 2n$; $0k0$: $k = 2n$; $00l$: $l = 2n$), though being smaller than 3σ, could be used for a more detailed analysis (Kirfel, 1994).

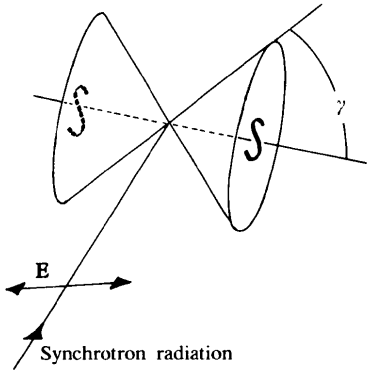

Figure 11
Anisotropic anomalous scattering from a disulfide bond (schematic), a model. The electrical vector, **E**, of the incident linearly polarized synchrotron radiation is in the z direction, whereas the direction of the S—S bond in general is different. The cone represents the emission of an electrical dipole, which is strongest in the plane orthogonal to the disulfide bond. The intensity of the emission is described by $a + b\cos^2\gamma$ (see text). A negative b means that the emission occurs preferentially in a direction orthogonal to the S—S bond. There is a maximum excitation of the S—S antenna when the electrical vector of the incident electromagnetic wave is parallel to it. For the calculation of the structure factor, all S—S bonds of the unit cell have to be considered.

12. Dispersion of the sulfate ions of the solvent

Trypsin crystals obtained from solutions of 2.5 M ammonium sulfate contain three times more sulfur as sulfate ions than sulfur in the amino acids of trypsin. There are 150 sulfate ions per unit cell compared with 56 S atoms of the four trypsin molecules. As the X-ray K-absorption edge of the sulfate ions is at shorter wavelengths, it will not obscure the dispersion of those S atoms which are part of trypsin (Fig. 1).

The 150 sulfate ions are almost randomly distributed in the solvent which occupies about 40% of the volume of the trypsin unit cell. Any change of the scattering factor of the sulfate ions due to the dispersion near the K-absorption edge would result in a change of the scattering density of the solvent. It is of interest to compare the electron density of the solvent with that of the protein. A 2.5 M solution of ammonium sulfate has an electron density of 0.384 e.u. $Å^{-3}$. A change of f' by 10 e.u. near the K-absorption edge of sulfate ions will lower the electron density to 0.368 e.u. $Å^{-3}$. These estimates hold at room temperature. In addition, an excess of the synthetic sugar Phytohistol (80%) as a cryoprotectant and the lower temperature will change the density of the solvent.

As the distribution of the solvent in the unit cell of trypsin is known, the structural information will be used to predict the anomalous dispersion of the diffracted intensity near the K-absorption edge of the sulfate ions. The calculation starts from the concept of the contrast which was introduced by Bragg & Perutz (1952) and which has been extended to anomalous dispersion (Fourme *et al.*, 1995). From a comparison of the dispersion of 90 reflections measured at five wavelengths (Fig. 1) with those calculated from the model, a small positive contrast of 0.03 e.u. $Å^{-3}$ is obtained. With an electron density of 0.42 e.u. $Å^{-3}$ of trypsin, the electron density of the solvent is 0.39 e.u. $Å^{-3}$.

The influence of the dispersion of the complex contrast on the scattering intensity will be demonstrated in the case of $F(\mathbf{h}) = F_{hkl} = F_{101}$. This reflection has by far the largest $|F|$, F_{000} excepted. In Fig. 12 the difference F_{101}(trypsin) − F_{101}(solvent) is shown in the plane of complex numbers. Both the minuend (= trypsin) and the subtrahend (= solvent) exhibit anomalous dispersion as described by (3). The experimental data in Fig. 12 clearly show the predominant dispersion of the sulfate ions which is much stronger than that of the other S atoms, as one would expect it to be at low structural resolution. The scattering factor of the solvent decreases at moderately high resolution, according to Porod's law, with $1/h^2$ (Fourme *et al.*, 1995) and its contribution to $I(hkl)$ becomes insignificant at $s > 0.2\,Å^{-1}$.

13. Conclusions

The anomalous dispersion of a larger number of reflections from trypsin agrees with that derived from the known model remarkably well. This is true for the application of both the MAD method relying on the S atoms of trypsin and the MASC method using the sulfate ions of the solvents. As the chemical states of the two kinds of S atoms are very different, the analysis of MAD does not interfere with that of MASC if the diffraction data are collected at wavelengths near the absorption edges. The *K*-absorption edge of the sulfate ions does not obscure the dispersion of the S atoms of trypsin (Fig. 1).

The technique of soft X-ray diffraction has seen considerable progress. The new vacuum-tight fast-mount sample cell is the result of a still continuing process of miniaturization. Using a Peltier cascade the protein crystal can be kept at 158 K during the diffraction experiment. The transparency of the X-ray beam path of the operational instrument has reached 20% for 5 Å radiation. The four area counters accept the diffracted intensity in a solid angle of $4\pi/10$. These developments were essential for the measurement of a larger number of reflections from single crystals of proteins.

In spite of the undeniable technical progress achieved, several improvements are desirable:

(i) A larger portion of the diffraction pattern should be recorded simultaneously. As the use of longer wavelengths will shift the diffraction peaks to larger angles, a cylindrical area detector covering a larger solid angle of diffracted intensity would mean an improvement with respect to the present detector system (Fig. 2). Imaging plates are flexible and therefore would lend themselves most easily to the construction of a wide-angle detector (Fig. 5). Their sensitivity to soft X-rays compares with that of MWPCs. The efficiency of imaging plates could probably still be increased by reducing the thickness of the protective layer of presently 10 μm (Amemiya, 1995).

(ii) Radiation damage is more severe with soft X-ray diffraction (Helliwell, 1992). As the surface suffers most from irradiation by soft X-rays, and as soft X-ray diffraction emerges essentially from the surface, it is this part of the crystal which needs to be protected by direct cooling. The conventional method of cooling by a cold nitrogen gas stream is the best choice, provided the coolant can be kept in the sample cell.

(iii) The presently used Peltier cascades are probably less useful as cooling of the crystal occurs from one side and the conduction of heat across the crystal may not be sufficient to maintain a reasonably uniform temperature.

(iv) Smaller protein crystals are preferred as they suffer less from any freezing procedure. Excellent results have been obtained from protein crystals with dimensions of less than 10 μm at high-brilliance synchrotron radiation sources (Xiao *et al.*, 1995; see also ESRF, 1996). These crystals are transparent even for soft X-rays.

(v) Sufficiently intense beams of soft X-rays are best obtained from undulators of modern synchrotron radiation sources. The beamline ID1 of the ESRF will be open for soft X-ray diffraction from 1998 onwards (Lequien, 1996). A considerable reduction of the beam time necessary for MAD measurements with sulfur and phosphorus is expected.

(vi) The presently planned cylindrical imaging-plate scanner with a built-in goniometer reduces the measuring time by an order of magnitude compared with the set of four MWPCs (Fig. 5) at constant radiation damage.

(vii) The improved performance of the detector system is of interest for MAD not only at the *K*-absorption edges of low-*Z* elements but also at the M_{IV}/M_V edges of elements heavier than rhenium (Z = 75), many of them exhibiting unusually strong anomalous dispersion.

(viii) The stability of the beam position and of the wavelength is of utmost importance for a reliable analysis of anomalous dispersion.

The latter point will certainly influence the progress of anomalous scattering in general and certainly that from proteins at wavelengths near the *K*-absorption edge of sulfur. A detailed analysis of anomalous dispersion not only separates sulfur in its extreme chemical states of −2 and +6, but it also could discriminate between sulfur in disulfide bridges from other S atoms of the amino acids cysteine and methionine (Fig. 1). This step is very desirable as it cuts down the number of S atoms contributing to a difference Patterson map (Stuhrmann, Bartels & Stuhrmann, 1997). Moreover, precision anomalous-dispersion experiments are

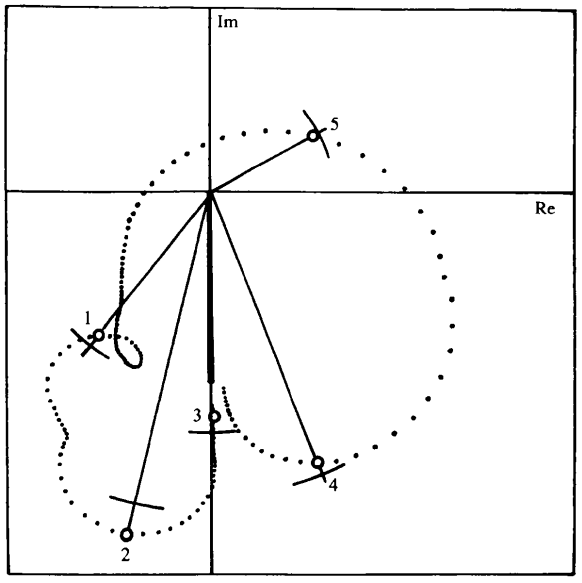

Figure 12
Argand diagram of F_{101}. Dots are calculated structure factors. The larger ones are the wavelengths which have been used in the experiment. The short sections of circles denote experimental values. The influence of the sulfate ions of the solvent as measured at wavelengths 4 and 5 on the dispersion of the total structure factor is stronger than that of the S atoms of the amino acids of the protein. At the low resolution of 43 Å corresponding to F_{101} the dispersion of the structure factor F_{101} closely resembles that of the complex contrast.

very likely to reveal the potential of anisotropic anomalous dispersion also in protein crystallography. It may even be very necessary in the analysis of anomalous dispersion of cystine.

The development of the soft X-ray diffraction technique received support from various sides. HASYLAB opened one of its beamlines for this purpose, implementing a double-mirror system and making it windowless by a differential pumping system. The European Molecular Biology Laboratory contributed its latest detectors and modified time digitizers. The fast data-storage system was built at the Physical Institute of the University of Hamburg. The glass capillaries were produced at the Institute of Inorganic Chemistry of the University of Hamburg. The smooth operation of the instrument would not have been possible without the technical help of Uwe Schulze. The analysis of the data in its final stage emerged from suggestions of Eric Fanchon at the Institut de Biologie Structurale, Grenoble. The Bundesministerium für Forschung und Technologie, Bonn, generously supported the initial stage of the project under grant Nos. 05294 SN and 05353 FA. We gratefully acknowledge the support from the Fonds der Chemischen Industrie.

References

Amemiya, Y. (1995). *J. Synchrotron Rad.* **2**, 13–21.
Balaic, D. X., Nugent, K. A., Barnea, Z., Garrett, R. & Wilkins, S. W. (1995). *J. Synchrotron Rad.* **2**, 296–299.
Bertrand, J. A., Auger, G., Fanchon, E., Martin, L., Blanot, D., van Heienoort, J. & Dideberg, O. (1997). *EMBO J.* In the press.
Bilderback, D. H., Thiel, D. J., Pahl, R. & Brister, K. E. (1994). *J. Synchrotron Rad.* **1**, 37–42.
Bode, W. & Huber, R. (1978). *FEBS Lett.* **90**, 265–269.
Boles, J. O., Lewinski, K., Kunckle, M. G., Hatada, M., Lebioda, L., Dunlap, R. B. & Odom, J. D. (1995). *Acta Cryst.* D**51**, 731–739.
Bragg, W. L. & Perutz, M. F. (1952). *Acta Cryst.* **5**, 277–289.
Crick, F. H. C. & Magdoff, B. S. (1956). *Acta Cryst.* **9**, 901–908.
Engström, P. & Riekel, C. (1996). *J. Synchrotron Rad.* **3**, 97–100.
ESRF (1996). *ESRF Highlights 1995/1996*, p. 54. ESRF, Grenoble, France.
Fanchon, E. & Hendrickson, W. A. (1990). *Acta Cryst.* A **46**, 809–820.
Fourme, R. & Hendrickson, W. A. (1990). *Biophysics and Synchrotron Radiation*, edited by S. S. Hasnain, pp. 156–175. Chichester: Ellis Horwood.
Fourme, R., Shepard, W., Kahn, R., l'Hermite, G. & Li de la Sierra, I. (1995). *J. Synchrotron Rad.* **2**, 36–48.
Harding, M. M. (1996). *J. Synchrotron Rad.* **3**, 250–259.
Helliwell, J. R. (1992). *Macromolecular Crystallography with Synchrotron Radiation*. Cambridge University Press.
Henderson, R. (1995). *Q. Rev. Biophys.* **28**, 171–193.
Hendrickson, W. A. (1991). *Science*, **254**, 51–58.
Hendrickson, W. A. (1994). *Resonant Anomalous X-ray Diffraction, Theory and Applications*, edited by G. Materlik, C. J. Sparks & K. Fischer, pp. 159–173. Amsterdam: Elsevier.
Hendrickson, W. A., Horton, J. R. & LeMaster, D. M. (1990). *EMBO J.* **9**, 1665–1672.
Hendrickson, W. A. & Teeter, M. M. (1981). *Nature (London)*, **290**, 107–113.
Hubbard, S. R., Greenall, R. J. & Woolfson, M. M. (1995). *Acta Cryst.* D**51**, 979–989.
Kirfel, A. (1994). *Resonant Anomalous X-ray Diffraction, Theory and Applications*, edited by G. Materlik, C. J. Sparks & K. Fischer, pp. 231–256. Amsterdam: Elsevier.
Lehmann, M. S., Müller, H.-H. & Stuhrmann, H. B. (1993). *Acta Cryst.* D**49**, 308–310.
Lequien, S. (1996). Personal communication.
Lewis, R. (1994). *J. Synchrotron Rad.* **1**, 43–53.
Marquardt, M., Walter, J., Deisenhofer, J., Bode, W. & Huber, R. (1983). *Acta Cryst.* B**39**, 480–490.
Otwinowski, Z. (1993). *MLPHARE. Isomorphous Replacement and Anomalous Scattering. Proceedings of the Study Weekend held at Daresbury Laboratory*, edited by W. Wolf, P. R. Evans & A. G. W. Leslie, pp. 80–86. SERC Daresbury Laboratory, Warrington WA4 4AD, UK.
Polikarpov, I. (1997). *J. Synchrotron Rad.* **4**, 17–20.
Popov, A. (1996). Personal communication.
Scholl, G., Dauvergne, F., Gabriel, A., Hütsch, M., Marmotti, M., Sayers, S., Stuhrmann, S., Thomas, J., Trame, C. & Stuhrmann, H. B. (1995). *Nucl. Instrum. Methods*, B**97**, 303–307.
Schwager, P., Bartels, K. S. & Jones, A. (1975). *J. Appl. Cryst.* **8**, 275–280.
SERC Daresbury Laboratory (1993). *CCP*4. *SERC Collaborative Computational Project in Protein Crystallography.* Version 2.2. SERC Daresbury Laboratory, Warrington WA4 4AD, UK.
Sheldrick, G. M. (1990). *Acta Cryst.* A**46**, 467–473.
Smith, J. L. (1991). *Curr. Opin. Struct. Biol.* **1**, 1002–1011.
Stuhrmann, H. B. (1982). *Makromol. Chem.* **183**, 2501–2514.
Stuhrmann. H. B., Goerigk, G. & Munk, B. (1991). *Handbook on Synchrotron Radiation*, Vol. 4, edited by S. Ebashi, M. Koch & E. Rubenstein, pp. 555–580. Amsterdam: Elsevier Science.
Stuhrmann, H. B. & Lehmann, M. S. (1994). *Resonant Anomalous X-ray Scattering, Theory and Applications*, edited by G. Materlik, C. J. Sparks & K. Fischer, pp. 175–194. Amsterdam: Elsevier Science.
Stuhrmann, S., Bartels, K. S., Hütsch, M., Marmotti, M., Sayers, Z., Thomas, J., Trame, C. & Stuhrmann, H. B. (1996). *Structural Studies of Crystals*, pp. 276–288. Moscow: Nauka Fizmatlit. (In Russian.)
Stuhrmann, S., Bartels, K. S. & Stuhrmann, H. B. (1995). *HASYLAB Annual Report II*, p. 807. HASYLAB, Hamburg, Germany.
Stuhrmann, S., Bartels, K. S. & Stuhrmann, H. B. (1997). *Z. Kristallogr.* **212**, 350–354.
Stuhrmann, S., Hütsch, M., Trame, C., Thomas, J. & Stuhrmann, H. B. (1995). *J. Synchrotron Rad.* **2**, 83–86.
Templeton, D. H. & Templeton, L. K. (1980). *Acta Cryst.* A**36**, 436–442.
Templeton, D. H. & Templeton, L. K. (1985). *Acta Cryst.* A**41**, 365–371.
Xiao, B., Smerdon, S. J., Jones, D. H., Dodson, G. G., Soneji, Y., Aitken, A. & Gamblin, S. J. (1995). *Nature (London)*, **376**, 188–190.